REVIEW

National Science Open
1: 20220031, 2022
https://doi.org/10.1360/nso/20220031

Information Sciences

Special Topic: Novel Optoelectronic Devices

Recent progress in graphene-based optical modulators on silicon photonics platform

Ciyuan Qiu, Huiying Zeng & Yikai Su*

State Key Lab of Advanced Optical Communication Systems and Networks, Department of Electronic Engineering, Shanghai Jiao Tong University, Shanghai 200240, China

*Corresponding author (email: yikaisu@sjtu.edu.cn)

Received 13 April 2022; Revised 6 August 2022; Accepted 19 August 2022; Published online 4 November 2022

Abstract: Graphene is a 2D material which has attracted tremendous interest from academia and industry, due to its attractive electrical and optical properties. By integrating graphene onto silicon photonics platform, various high-performance electro-optic and thermo-optic modulators have been demonstrated. In this paper, such graphene-based optical modulators are reviewed. The concept and principle of optical modulations are firstly analyzed and then an overview of the developing trends of optical modulators is presented. Meanwhile, the performances of graphene-based optical modulators, including power consumptions and speeds of electro-optic modulators as well as tuning efficiencies of thermo-optic modulators, are then evaluated and discussed in detail. All these optical modulators would play important roles in a wide range of applications including telecom, interconnects, computing, quantum information processing, and beam steering.

Keywords: optical modulator, graphene, integrated, high-speed

Introduction

Optical modulators are key components in the optical communication and optical computing systems [1–3]. By employing optical modulators, electrical signals can be converted to optical signals, which can thus be used for telecom, optical signal processing, optical computing, etc. To increase the capacities of optical systems and implement complex functions, large-scale integrated photonic circuits with high levels of integration are needed, in which high-performance integrated optical modulators are required. To obtain high-performance photonic circuits, integrated optical modulators with high speeds, low power consumptions, and high modulation efficiencies are highly desired.

Silicon photonics is considered an ideal platform for on-chip integration, owing to the advantages of compact footprint, low power consumption, and compatibility with complementary metal-oxide-semiconductor (CMOS) processes [4–10]. With rapid developments of silicon photonics, various silicon/silicon nitride-based integrated devices on the silicon photonics platform have been demonstrated [11–13]. Silicon nitride-based integrated devices on the silicon photonic platform are usually built with a silica buffer layer on a silicon wafer. By using carrier-plasma dispersion effect of silicon, high-speed electro-optic (EO) mod-

ulators can be realized [14–16]. Moreover, high tuning efficiency thermo-optic (TO) modulators can also be fabricated by using the TO effect of silicon or silicon nitride [17–20]. However, based on silicon photonic technology, it is still a challenge to build high-performance integrated EO/TO modulators with ultra-low power consumptions, ultra-high speeds, and high modulation efficiencies.

Graphene, a single sheet of carbon atoms in a hexagonal lattice, has attracted tremendous interest due to its attractive electrical and optical properties [21–30]. Graphene has an ultra-high carrier mobility of ~200,000 $cm^2\ v^{-1}\ s^{-1}$ at room temperature [31] and ultra-broadband optical absorption [32]. Moreover, the Fermi level of graphene (E_f) can be tuned through electric gating. Thus, by integrating graphene onto silicon photonics platform, ultra-high speed EO modulators could be built [33–35]. Meanwhile, monolayer graphene also has a low optical absorption of 2.3% for normal incident light [36]. Then, it can directly contact integrated waveguides. Furthermore, graphene has a high thermal conductivity of up to 2000 $W\ m^{-1}\ K^{-1}$. Thus, graphene-based micro-heaters can be used to build high-efficiency integrated TO modulators on silicon photonics platform [37–39].

In this review, we present a review of the current developments of near-infrared (NIR) integrated graphene-based optical modulators on silicon photonics platform and also indicate their developing trends in the near future [26,34,35,37–66]. This review is organized as follows. The Materials section focuses on the material properties. Next, the working principles of graphene-based optical modulators are analyzed. Then, integrated graphene-based EO/TO modulators are discussed. Conclusion and perspective are presented in the last section.

Materials

Silicon (Si), silicon nitride (Si_3N_4) and silica (SiO_2)

To realize integrated waveguides and then build optical devices, various materials have been used on silicon photonics platform. The bandgap of silicon, silicon nitride, and silica is 1.1, 5.3 and 9 eV, respectively, which are larger than the photon energy in the near infrared range (E_p=0.86 eV at 1550 nm). Then, they would have low optical absorption losses in the communication band. Moreover, all these three materials are compatible with the CMOS fabrication process and capable for large-scale device integration. Thus, silicon, silicon nitride, and silica are always used as basic materials for integrated photonic circuits. Their material properties are provided in Table 1 [67–75].

In the photonic circuit on silicon photonics platform, integrated waveguides are usually introduced based on silicon and silica. Silicon has a high refractive index of ~3.467, and silica has a low refractive index of 1.444. Thus, by using silicon as the waveguide core material and silica as the waveguide cladding material, the optical power can be confined in the waveguide core and a low propagation loss of ~4 $dB\ cm^{-1}$ could be obtained [67]. Meanwhile, to obtain electro-optic tuning, the refractive index of silicon can be tuned through carrier-plasma dispersion effect [76]. Moreover, silicon also has a strong thermo-optic effect with a TO tuning efficiency of $1.86\times10^{-4}\ K^{-1}$ [68]. Thus, one can build active optical modulators based on the EO and TO effects of silicon. However, the carrier mobility of silicon is only 1350 $cm^2\ v^{-1}\ s^{-1}$ [69] and the thermal conductivity of silicon is 80 $W\ m^{-1}\ K^{-1}$, which would limit their device performances in optical modulations.

To reduce the optical transmission loss, one can use silicon nitride as the waveguide core material and use

Table 1 Electrical and optical properties of silicon, silicon nitride, and silica

Material	Refractive index	Bandgap (eV)	TO coefficient (K^{-1})	Thermal conductivity (W m^{-1} K^{-1})	Carrier mobility (cm^2 v^{-1} s^{-1})	Propagation loss (dB cm^{-1}) [a]
Silicon [67–69]	3.467	1.1	1.86×10^{-4}	80	1350	4
Silicon nitride [70–73]	~2.0	5.3	2.5×10^{-5}	20	–	0.06
Silica [71,74,75]	1.444	9	0.95×10^{-5}	1.38	–	0.02[b]

a) Propagation loss of integrated waveguides. In such waveguides, the corresponding material in the table is used as the waveguide core material and silica is used as the cladding material. b) Extra doping process is required for the silica waveguide core. Thus, silica waveguide is usually not utilized on silicon photonics platform.

silica as the waveguide cladding material. Since silicon nitride has a low refractive index, the size of the silicon nitride waveguide would be relatively large. Meanwhile, the power confinement of silicon nitride waveguide would be a little lower than that of silicon waveguide. With a waveguide dimension of 2.8 μm and 100 nm, a low propagation loss of ~0.06 dB cm^{-1} has been obtained for a silicon nitride waveguide [70]. However, silicon nitride is an insulator material and does not have free carriers. Thus, it could not be directly used in the electro-optic modulation. Meanwhile, the thermo-optic effect and the thermal conductivity of silicon nitride are relatively low [71], as shown in Table 1. Thus, to implement optical modulators on Si_3N_4 waveguides, new materials should be introduced, especially for high-speed EO modulators.

Graphene

Graphene is a sheet of carbon atoms in a hexagonal lattice with photon-like massless and gapless electrons, as shown in Figure 1A [24,77]. Owing to the gapless linear dispersion of Dirac electrons in graphene, it has a wide-band operating spectral range [78]. Meanwhile, the Fermi level of graphene can be tuned through electrical gating [79,80]. Moreover, as shown in Figure 1B, the interband absorption can be blocked from Pauli blocking when $2E_f>E_p$ is satisfied. Here, $E_p=\hbar\omega$ is the photon energy, which is 0.86 eV at 1550 nm. Thus, in the communication band, the optical absorption can be suppressed if E_f is larger than 0.43 eV. Meanwhile, the carrier mobility and thermal conductivity of graphene are ~200,000 cm^2 v^{-1} s^{-1} and ~2000 W m^{-1} K^{-1}, respectively. With such a high carrier mobility and a high thermal conductivity, graphene

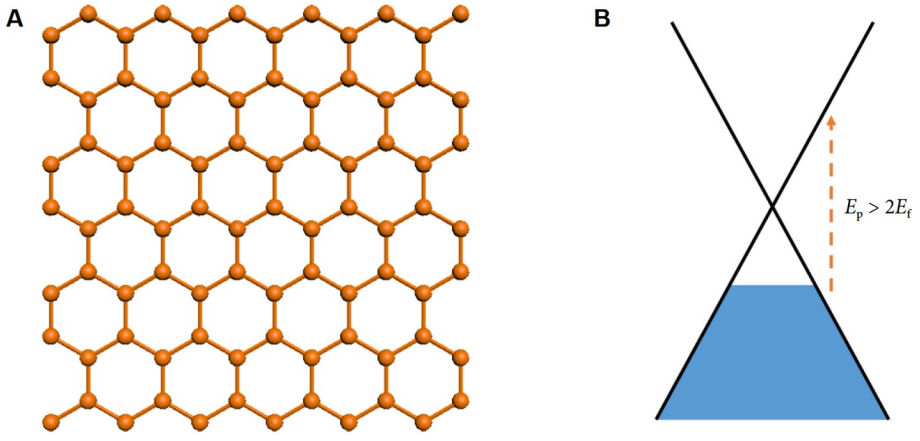

Figure 1 (A) Two-dimensional honeycomb structure of carbon atoms in graphene; (B) schematic diagram of possible interband optical transitions in graphene.

can thus be used in high-speed EO and TO modulations. However, since the thickness of graphene is only ~0.5 nm, the light-graphene interaction is low. Thus, to build integrated optoelectronic devices, graphene should always be integrated on optical waveguides to enhance the light-graphene interaction.

Principle of graphene-based optical modulators

Hybrid waveguide structure and optical properties

Based on the aforementioned material properties of silicon and silicon nitride on silicon photonics platform, one can find that new materials should be introduced to improve device performances of silicon and silicon nitride optical modulators. Meanwhile, graphene has promising properties to solve this issue. Thus, high-performance integrated optical modulators based on graphene-silicon and graphene-Si_3N_4 hybrid waveguides have been constructed.

Before discussing principles of the EO and TO modulations, we first analyze the electrical field distribution of a typical graphene-silicon hybrid waveguide as shown in Figure 2A. The dimension of the silicon waveguide is 500 nm×220 nm. The thickness of the Al_2O_3 and graphene is set to 7 and 0.5 nm, respectively. Meanwhile, the thickness of buried oxide (BOX) is 2 μm while the top cladding is air. Here, the permittivity of graphene is set to be 3.460+5.95*i* with a fermi level of 0.4 eV [33,81]. Then, as shown in Figure 2B, most of the optical power is confined in the silicon core and ~0.07% light power is evanescently coupled to the graphene layer. In such hybrid graphene-silicon waveguide, the propagation loss is ~200 dB cm^{-1} for the TE mode polarization [35]. The loss of such hybrid waveguide is polarization-dependent, which can be used for polarizers [82–84]. Here we use a typical graphene-silicon hybrid waveguide to analyze the electrical field distribution while the structure parameters of the waveguide can be modified for different applications in optical modulations.

Moreover, the propagation loss of the graphene-silicon waveguide can be decreased by lowering the optical power located in the graphene layer. This can be realized through enlarging the dimension of the waveguide or introducing a thick spacer material (i.e., Al_2O_3) between the graphene and silicon [37]. With such configurations, the light power in the graphene layer can be decreased. Then, the power ratio between the optical power in the graphene layer and the total optical power in the waveguide would be reduced. The imaginary part of the effective index of the graphene-silicon waveguide can be decreased, which depends on

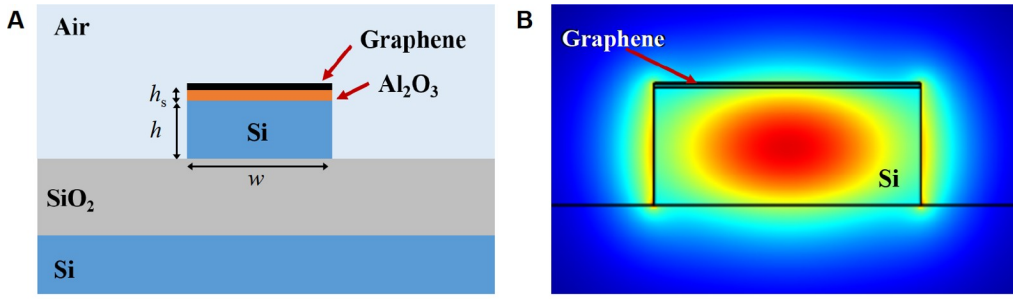

Figure 2 (A) Crosssection of a graphene-silicon hybrid waveguide; (B) electric field distribution profile of the TE fundamental mode. The waveguide width (w) is 500 nm and the waveguide height (h) is 220 nm. Al_2O_3 is the spacer material with a height (h_s) of 7 nm.

the energy ratio [85]. Since the imaginary part of the effective index determines the propagation loss, the loss induced by graphene could then be suppressed [86,87]. In this way, the quality factor for the graphene-silicon based resonator could be increased. However, the modulation efficiency would also be decreased. Thus, there is a tradeoff between the waveguide loss and the modulation efficiency for optical modulators based on such a hybrid waveguide configuration.

Furthermore, beside the structure of the graphene-silicon hybrid waveguide shown in Figure 2A, the silicon waveguide core could also be covered by silica, which is used to obtain a flat surface [48]. In that structure, silica is deposited by plasma enhanced chemical vapor deposition (PECVD) after the silicon waveguide fabrication. Then, silica cladding is planarized to the top surface of the waveguide based on standard chemical mechanical planarization (CMP) techniques. Thus, a flat surface can be provided before graphene transfer, which can protect graphene in the fabrication process. It should be noted that such a structure would only slightly affect the electrical field distribution and the modulation efficiency.

Based on such aforementioned hybrid waveguide structures, optical modulators can be built. In those modulators, optical modulations can be obtained by changing the effective index of the waveguides. In the EO modulation, the effective index of the waveguide can be tuned through changing the fermi level of graphene. In the TO modulation, with an applied heating power in the graphene layer, the silicon core will be heated and then the effective index of the waveguide can be changed. Here, the intrinsic speed of the EO modulation is >1 GHz, which is much faster than that of the TO modulation ~KHz. Detailed principles of EO and TO modulations will be presented in the next two sub-sections.

Electro-optic modulation

In the near-infrared region, based on the random phase approximation and the Kramers-Kronig relation, the gate-dependent permittivity of graphene has been extensively studied, which can be expressed as follows [33,81]:

$$\varepsilon_g{}'(E_p) = 1 + \frac{e^2}{8\pi E_p \varepsilon_0 d}\ln\frac{(E_p+2|E_f|)^2+\Gamma^2}{(E_p-2|E_f|)^2+\Gamma^2} - \frac{e^2}{\pi\varepsilon_0 d}\frac{|E_f|}{E_p^2+(1/\tau)^2}, \tag{1}$$

$$\varepsilon_g{}''(E_p) = \frac{e^2}{4E_p\varepsilon_0 d}\left[1+\frac{1}{\pi}\left(\tan^{-1}\frac{E_p-2|E_f|}{\Gamma} - \tan^{-1}\frac{E_p+2|E_f|}{\Gamma}\right)\right] + \frac{e^2}{\pi\tau E_p\varepsilon_0 d}\frac{|E_f|}{E_p^2+(1/\tau)^2}, \tag{2}$$

where $\varepsilon_g{}'$ and $\varepsilon_g{}''$ are the real part and imaginary part of the permittivity, respectively. Meanwhile, d is the thickness of graphene, which is set to 0.5 nm. Γ is the interband linewidth broadening, which is set to 110 meV. In the equation, the free carrier scattering rate $1/\tau$ can be neglected since it is much smaller than the incident photon energy. Figure 3A shows the real part and imaginary part of the permittivity under different Fermi levels. Here, the light wavelength is set to 1550 nm. One can find that the real part reaches its maximum when the Fermi level is 0.4 eV. Meanwhile, when the Fermi level increased to be larger than 0.49 eV, the real part would be less than 0. This indicates that graphene has metallic properties. Moreover, when the Fermi level increases from 0 to 1 eV, the interband absorption is suppressed due to the Pauli blocking. Then, the imaginary part of graphene decreases if the Fermi level increases.

Based on the gate dependent permittivity of graphene, the effective index of the hybrid waveguide shown in Figure 2A can be calculated. As shown in Figure 3B, the effective modal index of the hybrid waveguide is

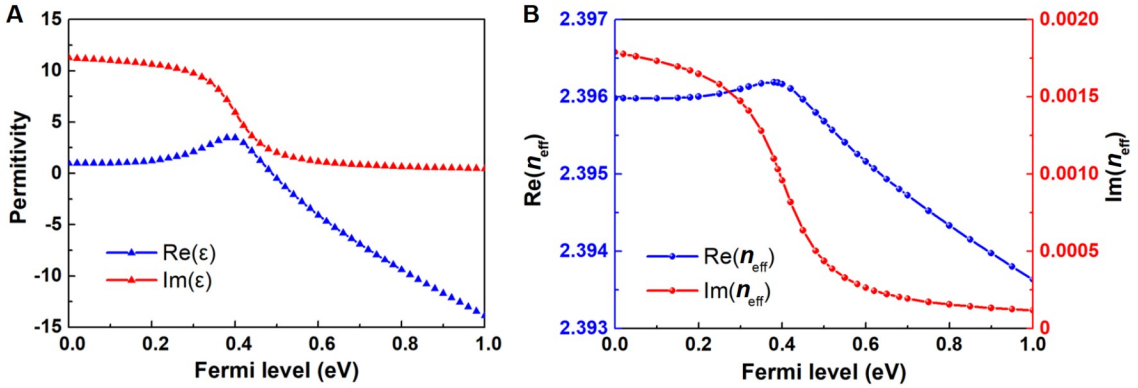

Figure 3 (A) Real part and imaginary part of the anisotropic in-plane permittivity of graphene under different Fermi levels. (B) Real and imaginary parts of effective modal index (n_{eff}) of a 500 nm×220 nm single-mode silicon waveguide as a function of the Fermi level.

changed with respect to the Fermi level. The real part of the effective index determines the phase change in the waveguide while the imaginary part determines the loss in the hybrid waveguide. Thus, by changing the Fermi level of graphene, the phase and the loss in the waveguide can both be changed, simultaneously. In this way, the EO modulation can be obtained. Moreover, a high modulation speed could be expected since graphene has a large carrier mobility of ~200,000 $cm^2\ v^{-1}\ s^{-1}$.

Here we use monolayer graphene to illustrate the principle of the EO modulation for the graphene-based modulators on silicon photonics platform. In such devices, graphene-silicon capacitors are formed. The Fermi level of graphene is usually tuned by applying gate voltage between the graphene and doped silicon [40]. Moreover, double-layer graphene modulators can also be implemented, in which a graphene-graphene capacitor can be built and the gate voltage is applied between two graphene layers. Then, the Fermi levels of the two graphene layers would be tuned in different directions. In this way, the permittivity of two-layer graphene can be changed and the EO modulation can also be obtained [43].

Thermo-optic modulation

In this sub-section, the concept for the graphene-based TO modulation on silicon photonics platform is evaluated based on the hybrid waveguide shown in Figure 2A. Here the spacer material (Al_2O_3) is not used. For a graphene-based TO modulator, the electrical power can be applied onto the graphene layer. The graphene layer can absorb the electrical power and convert it to heat. Then, the graphene layer can work as a micro-heater and heat the integrated waveguide underneath. For such a graphene-silicon hybrid structure, the 2D temperature distribution is shown in Figure 4. In the simulation, the thermal conductivities of silicon, silicon oxide, and graphene are set to ~80, ~1.38, and ~2000 $W\ m^{-1}\ K^{-1}$, respectively. The heat convection coefficient of air is set to 5 $W\ m^{-2}\ K^{-1}$. When the thermal energy density (Q) in the graphene layer is set to $6\times10^{16}\ W\ m^{-3}$, the temperature of the silicon waveguide increases by ~10 K. Since the TO coefficient of silicon is $dn/dT=1.86\times10^{-4}\ K^{-1}$, the refractive index of silicon can then increase. Thus, the effective index of the graphene-silicon waveguide (n_{eff}) can be tuned. The real part of n_{eff} determines the waveguide phase delay and the imaginary part affects the loss. Thus, the TO modulation based on a graphene heater can then be obtained.

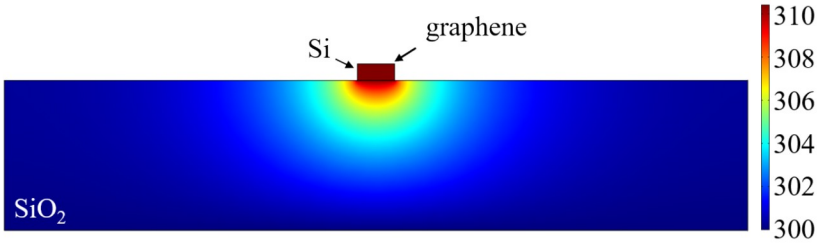

Figure 4 2D temperature distribution of a hybrid graphene-silicon waveguide. The silicon waveguide has a dimension of 500 nm×220 nm. The thickness of graphene is 0.5 nm. Moreover, the spacer material is not used here and h_s is set to 0.

State-of-the-art of graphene-based optical modulators

This section reviews recent developments of graphene-based EO/TO modulators on silicon photonics platform, by using principles discussed above. For the EO modulation, the chip-integrated EO modulators and free-space optical modulators will be presented. The modulation depths, modulation speeds, and power consumption will be evaluated. For the TO modulation, waveguide-coupled optical modulators will be discussed, in which the TO tuning efficiencies and thermal responses would be elaborated. All those integrated devices work in the communication band.

Chip-integrated EO modulators

Chip-integrated EO modulators are key components for the on-chip optical interconnects. To obtain high-performance photonic circuits, modulation speeds and power consumption are key parameters for such devices. In the following sub-sections, various graphene-based chip-integrated modulators are presented. All those modulators follow the principle of the EO modulation discussed above.

Waveguide-coupled optical modulators

For waveguide-coupled optical modulators, monolayer graphene-based optical modulators have attracted much attention from researchers. As shown in Figures 5A–5C, Liu *et al*. [40] demonstrated the first electro-absorption optical modulator in 2011. In that device, the chemical vapour deposition (CVD) grown graphene is used and mechanically transferred onto the silicon waveguide. The length of the graphene-silicon hybrid waveguide is set to 40 μm and the thickness of Al_2O_3 is 7 nm. By applying gate voltage between the graphene and doped silicon, the Fermi level of graphene can be tuned. Then, the optical modulation can be obtained with a modulation efficiency of ~0.1 dB μm^{-1} while the modulation bandwidth is 1.2 GHz. To meet the requirement of optical communication systems, the performances of monolayer graphene-based optical modulators are further improved [34,41,42]. In 2016, Hu *et al*. [41] built a high-speed electro-absorption modulator, as shown in Figures 5D–5F. In that device, the insertion loss is 3.8 dB and the modulation depth is ~5.2 dB, by optimizing the device design and fabrication process. Meanwhile, the series resistor is reduced to 241 Ω and the capacitor is about 80 fF. Then, a modulation speed of 10 Gb s^{-1} is obtained with a 3-dB bandwidth of 5.8 GHz. Moreover, the power consumption is about 350 fJ bit^{-1}.

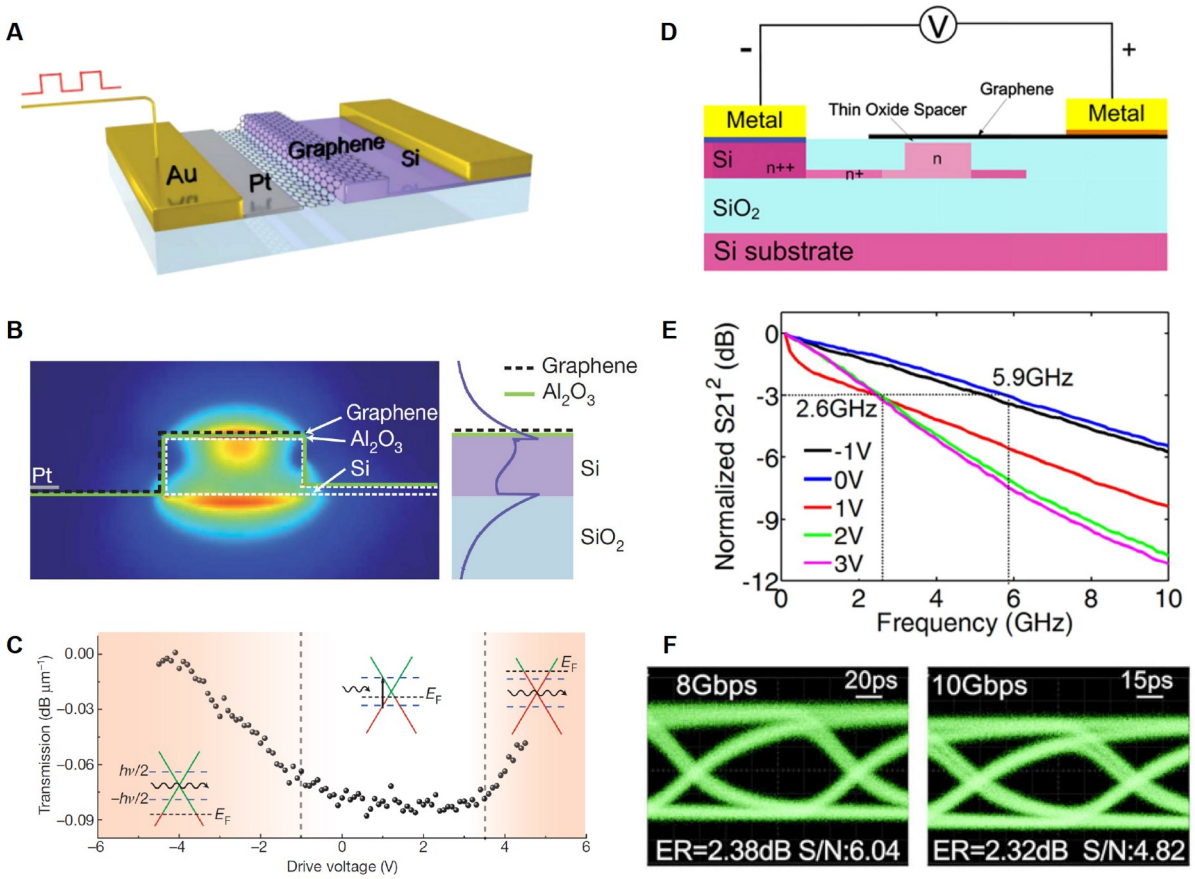

Figure 5 Chip-integrated monolayer graphene EO modulators. (A) Schematic illustration of a graphene-based optical modulator; (B) electrical field distribution of the hybrid graphene-silicon waveguide; (C) static EO response of the device [40]; (D) diagram of a high-speed EO modulator with a speed of 10 Gb s^{-1}; (E) measured and normalized EO S_{21} responses; (F) optical eye diagrams at 8 and 10 Gb s^{-1} modulation speeds [41]. (A)–(C) Adapted with permission from [40]. Copyright 2011, Springer Nature. (D)–(F) Adapted with permission from [41]. Copyright 2016, WILEY-VCH.

To increase the modulation efficiency, double-layer graphene electro-absorption modulators are implemented. As shown in Figures 6A–6C, a double-layer graphene-based optical modulator was demonstrated in 2012 [43]. In that device, the capacitor is formed by a graphene-SiN/hBN-graphene structure. The Fermi levels of both two graphene layers can be tuned, as shown in Figure 6C. The modulation efficiency of the device is about 0.16 dB μm^{-1} which is twice as high as that of the monolayer graphene-based optical modulator [40]. Moreover, the 3-dB bandwidth is about 1 GHz, which is limited by the high series resistance of ~1 kΩ in the device fabrication process. Then, to improve the modulation speed, several approaches have been proposed and demonstrated [44–47]. In 2019, Giambra *et al*. [47] demonstrated a high-speed double-layer graphene-based optical modulator, as shown in Figures 6D–6F. The device length is optimized to be 120 μm and the modulation efficiency is about 0.137 dB μm^{-1}. To reduce the series resistance, top contacts are made of a stack of Nickel (Ni) and Gold (Au). Then, the contact resistance is reduced to about <10 Ω. Meanwhile, the electrical capacitor is 204 fF. Thus, the 3-dB bandwidth is about 29 GHz. Furthermore, a modulation speed of 50 Gb s^{-1} is obtained with an extinction ratio (ER) of 1.3 dB, as shown in the eye diagram.

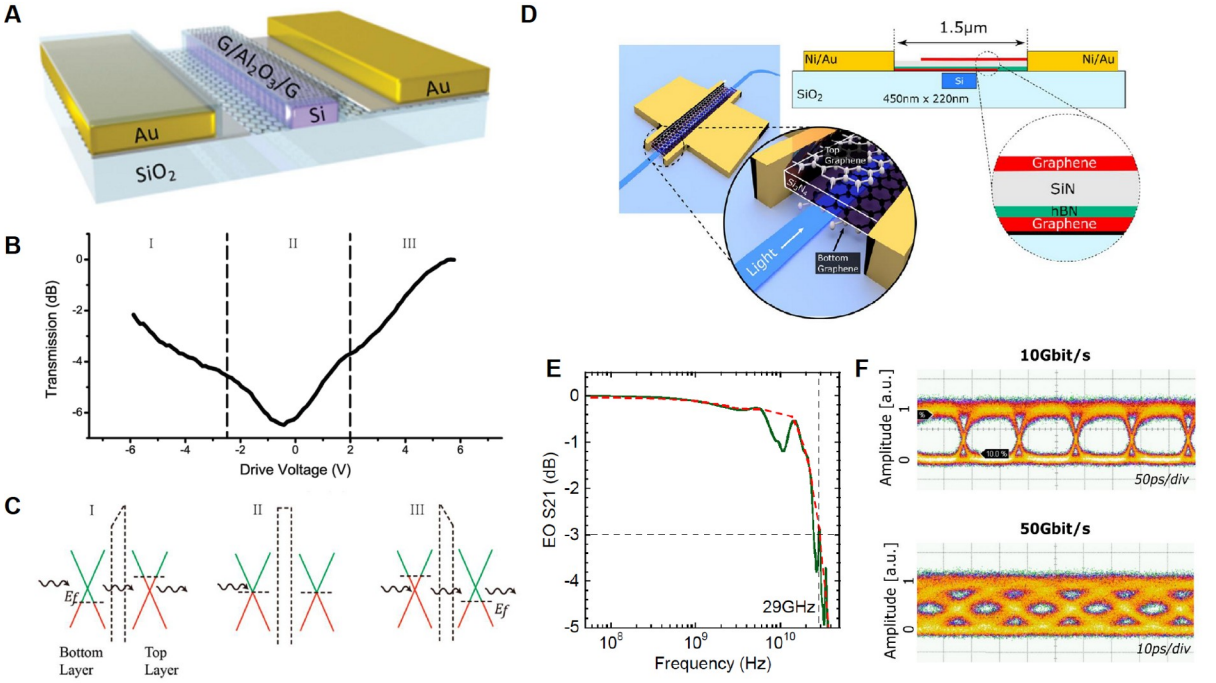

Figure 6 Chip-integrated double-layer graphene EO modulators. (A) Schematic illustration of a double-layer graphene modulator; (B) static response of the modulator; (C) the graphene band profiles (green for unoccupied state, red for occupied states) for regions I, II, and III in (B) [43]; (D) diagram of a high-speed double-layer graphene modulator; (E) EO S_{21} bandwidth of the double-layer graphene optical modulator; (F) eye diagrams at data rates of 10 and 50 Gb s^{-1} [47]. (A–C) Adapted with permission from [43]. Copyright 2012, American Chemical Society. (D–F) Adapted with permission from [47]. Copyright 2019, Optica publishing group.

Waveguide-coupled phase modulators

Graphene can also be used to build the optical phase modulators. As shown in Figure 3B, the imaginary part of the effective index is relatively small, when E_F>0.4 eV. This indicates that the loss of the hybrid waveguide is low. In this condition, the real part of the effective index of the hybrid graphene-silicon waveguide can be effectively tuned. Then, a strong phase modulation can be obtained.

A graphene-silicon high-speed phase modulator was first demonstrated in 2018 [48]. In that device, monolayer graphene is integrated onto both two arms of the Mach-Zehnder interferometers (MZI) structure, as shown in Figure 7. The length of the phase-shifter is 300 μm and the extinction of the modulator is about 35 dB. Meanwhile, graphene is gated beyond the Pauli blocking condition (E_f>0.4 eV at 1.55 μm), and the device then operates in the low-loss region. Thus, the phase modulation is dominant with respect to amplitude changes. The modulation efficiency of the phase shifter is measured to be about 0.28 V cm at 1550 nm. Moreover, with 2-V_{pp} driving voltage in a push-pull configuration, the device can operate at a speed of 10 Gb s^{-1} with an EO bandwidth of 5 GHz. The fabrication process of the graphene-based phase modulators is similar to those of the abovementioned graphene-based amplitude modulators. Furthermore, to improve the device performance, several schemes have been proposed recently [88–90]. Within a proposed structure shown in Figure 7C, Ye *et al*. [88] theoretically predicted that the 3-dB bandwidth of a graphene-based phase modulator can approach 119.5 GHz.

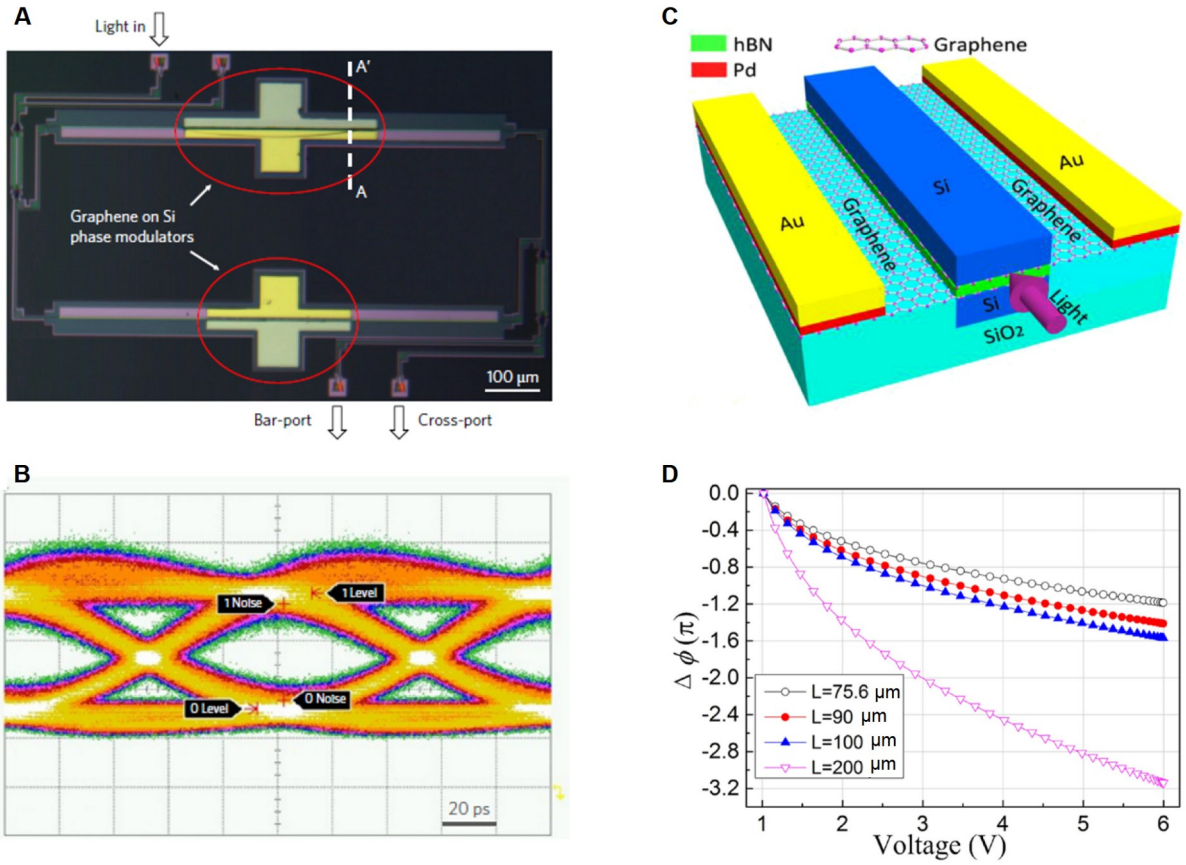

Figure 7 (A) Optical micrograph of a graphene phase modulator based on Mach-Zehnder interferometer. (B) Eye diagram at 10 Gb s^{-1} [48]. (C) 3D view of an optical phase modulator based on a graphene-silicon hybrid waveguide. (D) Phase change curves under different applied voltages [88]. (A) and (B) Adapted with permission from [48]. Copyright 2018, Springer Nature. (C) and (D) Adapted with permission from [88]. Copyright 2017, IEEE.

Resonator-coupled optical modulators

To reduce the size of the device and increase the modulation depth, ring-coupled optical modulators are implemented. In 2014, Qiu *et al*. [35] demonstrated an optical modulator with gated graphene on a silicon micro-ring resonator. In that device, monolayer graphene is transferred onto the silicon-micro ring resonator. By tuning the Fermi level through electric gating, a ~40% amplitude modulation depth is obtained. In 2015, to enhance the modulation depth, Ding *et al*. [49] demonstrated a novel graphene-silicon micro-ring modulator, as shown in Figures 8A and 8B. In that device, a large power coupling coefficient is obtained by using a small coupling gap of ~150 nm. Meanwhile, the graphene coverage of ~25% on the ring waveguide is also promptly selected. Thus, the device initially works in slightly under-coupling condition and in critical coupling after tuning graphene. In this way, the modulation depth is enhanced to be 12.5 dB.

To further improve the speed of such micro-ring modulators, Phare *et al*. [50] demonstrated a high-speed micro-ring modulator based on graphene-Si_3N_4 hybrid waveguides. By using double-layer graphene, the graphene-graphene capacitor can be formed and the Fermi level of the graphene can be effectively changed. As shown in Figures 8C and 8D, a 22 Gb s^{-1} non-return-to-zero eye diagram is measured while the 3-dB

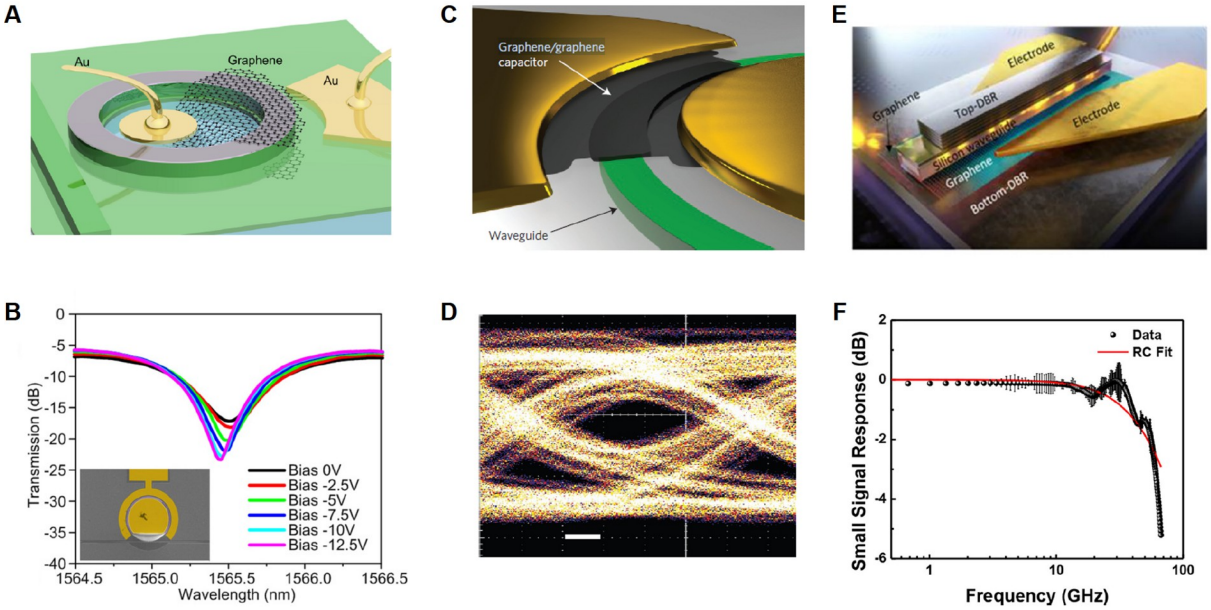

Figure 8 (A) Schematic diagram of a graphene-silicon microring modulator. (B) Measured transmission spectra at different voltages [49]. (C) Diagram of a graphene-Si_3N_4 micro-ring modulator. (D) Eye diagram at 22 Gb s^{-1} [50]. (E) Schematic illustration of a graphene-based optical modulator using a Bragg reflector waveguide. (F) RF response of the double-layer graphene-based optical modulator [52]. (A) and (B) Adapted with permission from [49]. Copyright 2015, American Chemical Society. (C) and (D) Adapted with permission from [50]. Copyright 2015, Springer Nature. (E) and (F) Adapted with permission from [52]. Copyright 2022, De Gruyter.

bandwidth is 30 GHz. The power consumption is about 800 fJ bit^{-1}, which is limited by the relatively large capacitance of ~55 fF and the series resistor of ~100 Ω. Such an optical graphene-Si_3N_4 micro-ring modulator also shows its high performance under a low temperature of ~4.9 K [51].

To effectively decrease power consumption, one could reduce the electrical capacitance by shrinking the device size. In 2022, Heidari *et al*. [52] demonstrated an ultra-low power graphene-based optical modulator by using a Bragg reflector waveguide. In that device, a Bragg reflector waveguide is laterally merged with a silicon waveguide. Then, slow light is formed by using the distributed Bragg reflector (DBR) structure and the light-matter interaction is greatly enhanced within a 10 μm-long waveguide. Moreover, the capacitor can be decreased to 27 fF. In the demonstration, the measured 3-dB bandwidth is 60 GHz while the power consumption is only 2.25 fJ bit^{-1}. Such a modulator is advantageous for ultra-dense on-chip optical communication applications.

Performance comparison

To clearly show the performance of the chip-integrated graphene-based optical modulators, a partial list of typical chip-integrated graphene-based optical modulators is provided in Table 2. One can clearly find that resonator-based optical modulators would have high modulation depths, relatively low power consumptions and large bandwidths. Meanwhile, for waveguide-coupled optical modulators, electrical capacitances could be relatively large [47], which are limited by the device lengths. Then, the modulation bandwidths of waveguide-coupled optical modulators would be restrained. Moreover, based on demonstrated optical

Table 2 A partial list of typical chip-integrated graphene-based optical modulators

Structure and reference	Layers of graphene	Insertion loss (dB)	Modulation depth (dB)	Bandwidth (GHz)	Power consumption (fJ bit^{-1})
Non-planarized Si waveguide [40]	Monolayer	–	4	1.2	–
Planarized Si waveguide [41]	Monolayer	3.8	5.2	5.9	350
Planarized Si waveguide [34,42]	Monolayer	4	4.5	5	–
Non-planarized Si waveguide [43]	Double-layer	4	6.5	1	–
Non-planarized Si waveguide [44]	Double-layer	3.3	16	0.67	–
Planarized Si waveguide [45]	Double-layer	–	0.5	2.5	–
Non-planarized a-Si waveguide [46][a)]	Double-layer	~1	2	35	1400
Planarized Si waveguide [47]	Double-layer	2.2	16	29	600
Planarized Si waveguide-MZI [48]	Monolayer	–	35	5	1000
Non-planarized Si waveguide-ring [35]	Monolayer	–	2.2	80[b)]	–
Non-planarized Si waveguide-ring [49]	Monolayer	~5	12.5	–	–
Planarized Si_3N_4 waveguide-ring [50]	Double-layer	–	15	30	800
Planarized Si_3N_4 waveguide-ring [51]	Double-layer	–	7	14.7	–
Non-planarized a-Si waveguide-DBR [52][a)]	Double-layer	–	~12	60	2.25

a) a-Si: amorphous silicon. b) Modulation bandwidth is obtained by calculation.

modulators, double-layer graphene-based optical modulators are preferred to obtain high-speed performances.

The device performances of the waveguide-coupled optical modulators might also be influenced by the fabrication process. For instance, after graphene transfer, broken area of graphene would exist and the initial fermi level of graphene cannot be controlled. Both these two factors could affect the loss from graphene. Thus, it could be difficult for resonator-coupled optical modulators to obtain high modulation depths and low insertion losses. Moreover, electrical capacitances would be relatively large for fabricated waveguide-coupled optical modulators, since their device lengths are usually longer than 100 μm. Such large capacitances would affect modulation speeds. Furthermore, compared with monolayer graphene EO modulators, double-layer graphene EO modulators can avoid the insertion loss from doped silicon. However, the mechanical transfer of the second graphene sheet is required for double-layer graphene modulators, which might increase the fabrication complexity and affect the device performances.

Free-space optical modulators

Free-space optical modulators can be used for high speed free-space optical communications, free-space optical computing, etc. [91]. Several silicon free-space optical modulators have been demonstrated, whose speeds, however, are relatively low (i.e., <150 MHz). By using the ultra-high carrier mobility of graphene, high-speed free-space modulations can be achieved by integrating graphene onto silicon optical devices. Moreover, in the mid-infrared range, a GHz spatial light modulator was demonstrated based on the graphene metasurface, in which a plasmonic resonance was formed [92]. Thus, GHz graphene-based near-infrared modulators could also be expected. Meanwhile, to obtain effective free space optical modulation, resonators should be introduced for near-infrared free-space optical modulators, since the optical absorption of monolayer graphene is only 2.3% for normal incident light.

To obtain free-space modulation, two free-space light modulators were demonstrated by Majumdar *et al*. [53] and Gan *et al*. [54], respectively. In these studies, normal incident light can be coupled into the photonic

crystal (PhC) cavity, based on a PhC cavity and a diffraction coupling scheme. Then, by tuning the Fermi level of graphene located on top of the PhC, the resonance wavelengths can be tuned by ~2 nm. High modulation depths of >6 dB can thus be achieved. However, in those two free-space modulators, the electrical capacitors are formed by ion-gel and thus the modulation speeds are limited.

To improve the modulation speed, Gao *et al*. firstly fabricated a high-performance modulator. As shown in Figure 9C, a BN/graphene/BN/graphene/BN five-layer stack is first prepared. Then, a silicon PhC membrance is transferred onto this stack [55]. In that device, the electrical capacitor is formed by a graphene-BN-graphene structure and thus a high speed can be achieved. The measured modulation depth is 3.2 dB and the bandwidth is ~1.2 GHz. Meanwhile, the capacitance of the device is 320 fF and the switching energy is approximately 1 pJ bit^{-1}. To improve the extinction ratio and the coupling efficiency, a high contrast grating (HCG) structure was utilized by Sun *et al*. [56]. In that device, graphene is transferred onto the HCG structure and the Fermi level of graphene can be tuned by using ion-gel. Then, a modulation depth of ~11 dB and a dynamic modulation speed of >1 MHz are obtained. Meanwhile, a graphene-based spatial light modulator was also obtained by using graphene/silicon nanohole array with a high modulation depth of >10 dB [57].

The performance parameters of the abovementioned free-space modulators are shown in Table 3. One can find that the modulation bandwidths of demonstrated devices would be lower than 1 MHz, if a top electrolyte gating with ion-gel is used [53,54,56,57]. However, their intrinsic bandwidths should be >1 GHz as the mid-infrared graphene-based modulator [92]. The bandwidths of those modulators can be increased by changing the gating schemes.

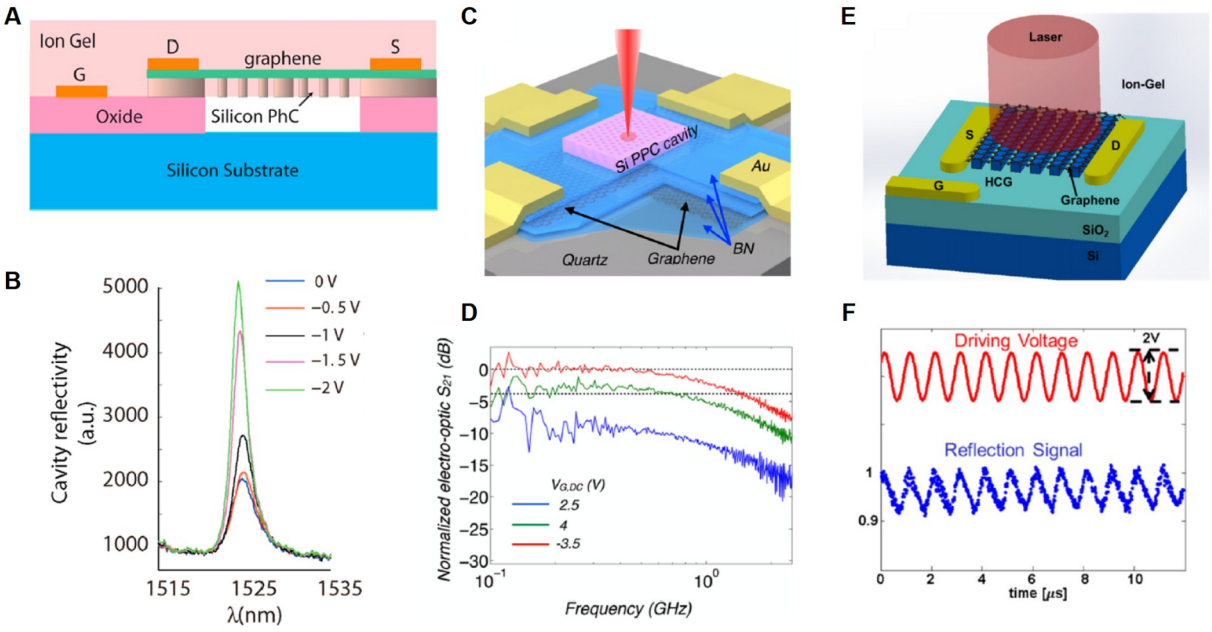

Figure 9 Graphene-based free-space optical modulators. (A) Schematic diagram of a graphene-PhC modulator. (B) Gate-voltage-induced differential reflection spectra at different voltages [53]. (C) Diagram of a cavity-graphene EO modulator. (D) Normalized EO S_{21} frequency responses at different DC gate voltages [55]. (E) Schematic of an HCG-graphene based spatial light modulator. (F) Reflection response at 1 MHz [56]. (A) and (B) Adapted with permission from [53]. Copyright 2013, American Chemical Society. (C) and (D) Adapted with permission from [55]. Copyright 2015, American Chemical Society. (E) and (F) Adapted with permission from [56]. Copyright 2016, Optica Publishing Group.

Table 3 A partial list of typical free-space graphene-based optical modulators

Structure and reference	Modulation depth (dB)	Bandwidth (MHz)	Power consumption (fJ bit^{-1})
Si photonic crystal cavity [53]	6	–	–
Si photonic crystal cavity [54]	>10	–	–
Si photonic crystal cavity [55]	3.2	1200	1000
Si high contrast grating [56]	11	1	–
Si nanohole array [57]	>10	0.001	–

Thermo-optic modulators

Thermo-optic modulators are quite useful in the data switching and tunble filters, in which low power is needed. For traditional integrated thermo-optic modulators, metal heaters are usually integrated. However, due to the strong optical absorption loss of metals, metal heaters cannot directly contact silicon waveguides. Thus, a buffer silica layer is usually introduced to reduce the propagation loss induced by metal layers. Then, in this way, the tuning efficiency would be decreased and the response time would be slow. Graphene has a much lower optical absorption compared with metals. Thus, graphene can directly contact with waveguides [93,94] and then increase the TO tuning efficiency. Meanwhile, the graphene has a large thermal conductivity, which can significantly improve the TO tuning speed.

Several graphene-based TO modulators have been demonstrated, as shown in Table 4. In 2015, Gan *et al*. [58] demonstrated a highly efficient TO micro-ring modulator assisted by graphene with a tuning efficiency of ~0.104 nm mW^{-1}, as shown in Figures 10A and 10B. To further increase the tuning efficiency, one needs to shrink the size of the resonator and then reduce the optical mode volume. By using a race-track resonator with a bending radius of 2.5 μm and straight portions of 3 μm, the mode volume can be effectively reduced. Then, a TO tuning efficiency of 0.24 nm mW^{-1} is obtained [59]. Meanwhile, a high-performance tunable silicon photonic microdisk resonator with a transparent graphene nanoheater was also demonstrated [60], as shown in Figures 10C and 10D. By using a micro-disk with a radius of 2 μm, a high tuning efficiency of 1.67 nm mW^{-1} is achieved. Furthermore, a graphene-based TO modulator was also implemented based on a slow-light silicon photonic crystal waveguide, in which the light matter interaction is enhanced, as shown in Figures 10E and 10F. In that device, a high tuning efficiency of 1.07 nm mW^{-1} is realized [38]. Moreover, based on a 1D PhC cavity with an ultrasmall mode volume, a tuning efficiency of 1.5 nm mW^{-1} was demonstrated. The response time for graphene-based TO devices is approximately 1 μs, which is much faster than those of metal-heater based TO devices. That should be attributed to the high thermal conductivity of graphene.

Furthermore, as mentioned above, the TO efficiency can be effectively enhanced when the graphene layer

Table 4 Recent progress of graphene-silicon TO devices

Structure and reference	Tuning efficiency (nm mW^{-1})	Response time (μs)	Spacer
Graphene on Si micro-ring [58]	0.104	0.75	No
Graphene on Si racetrack-type resonator [59]	0.24	1.2	No
Graphene on Si micro-disk [60]	1.67	12.8	No
Graphene on Si PhC [38]	1.07	0.75	No
Graphene on Si nanobeam [39]	1.5	1.47	No
Graphene on Si micro-ring [37]	0.33	3	Yes

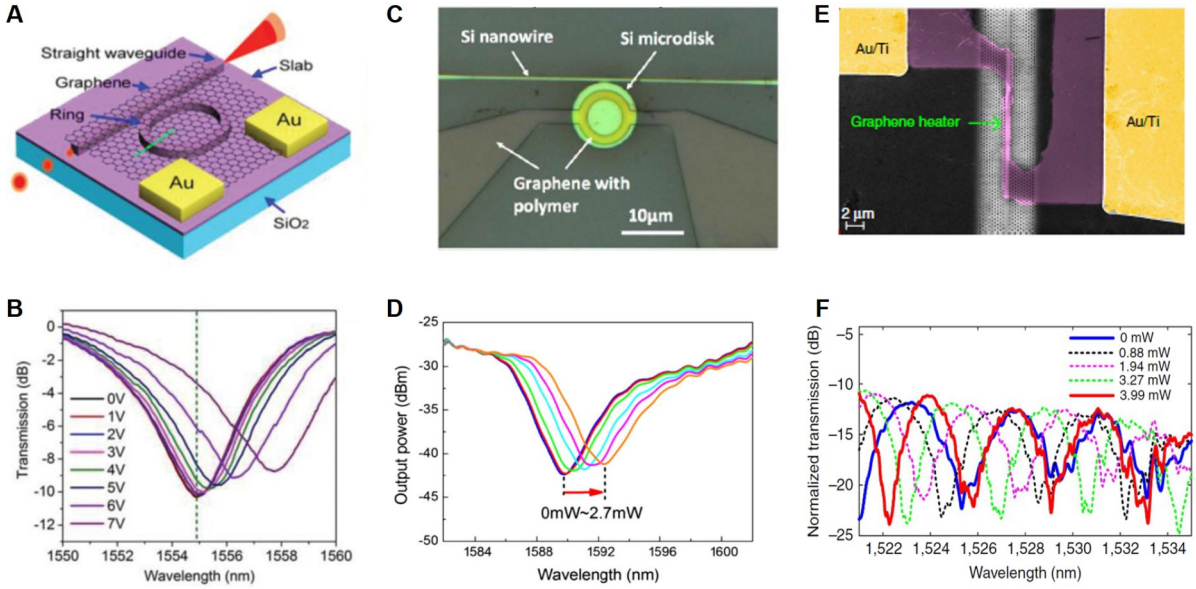

Figure 10 Graphene-based TO modulators. (A) 3D illustration of a graphene-based TO microring modulator. (B) Transmission spectra of the ring resonator at different drive voltages [58]. (C) Microscope image of a graphene-based TO microdisk modulator. (D) Spectral responses of the thermally tunable microdisk resonator as a function of the heat power [60]. (E) Colour scanning electron microscope image of a TO modulator based on slow-light-enhanced graphene micro-heater. (F) Static response of the heating power [38]. (A) and (B) Adapted with permission from [58]. Copyright 2015, Royal Society of Chemistry. (C) and (D) Adapted with permission from [60]. Copyright 2016, Optica Publishing Group. (E) and (F) Adapted with permission from [38]. Copyright 2017, Springer Nature.

directly contacts with the micro-resonators. However, the extinction ratio and quality factor of these resonators would also be degrated due to the loss from graphene. To solve this issue, a spacer based on hydrogen silsesquioxane (HSQ) and Al_2O_3 is introduced between the graphene layer and the silicon waveguide [37]. The height of the spacer is about 240 nm. Then, the loss induced by graphene can be reduced. In the experiment, the tuning efficiency is measured to be 0.33 nm mW^{-1} and the response time is ~3 μs.

Conclusion and perspective

In this review, we review the recent progress in the NIR graphene-based EO/TO optical modulators on silicon photonics platform. All these demonstrations show that graphene is a promising material to build high-speed and low-power optical modulators. In the future, to further reduce EO power consumption of chip-integrated optical modulators, graphene should be integrated onto ultra-compact resonators to reduce the electrical capacitances [95,96]. Meanwhile, to obtain ultra-fast speed modulators, series resistors should be decreased by optimizing the fabrication process. In this way, chip-integrated high-speed EO modulators with a modulation speed of >100 GHz [33,95] and a power consumption of <1 fJ bit^{-1} could be obtained [26]. Moreover, graphene is also an ideal material for the free-space light modulation. Inspired by the demonstration in the mid-infrared, high-speed near-infrared free space optical modulators could also be realized by using novel resonators and graphene. Such GHz free-space modulators could be very useful in spatial light communication, beam steering, optical communication, etc. For thermo-optic modulators, tuning efficiencies could be improved by enhancing the graphene-light interactions. In this way, a tuning efficiency of >3 nm mW^{-1}

could be implemented [39]. In addition, future challenges for high-performance graphene-based optical modulators may lie in practical issues in mass production [65]. For on-chip integration of graphene-based optical modulators, it is still a big challenge to obtain large, uniform, and high-quality graphene. Moreover, to obtain high device performance uniformity, controllable and stable chemical doping for the graphene sheets is highly required. Furthermore, in practical application, there is still a significant need for better metal contacts and compatible insulators. All these challenges could in turn bring great opportunities and become the new driving force to improve the device performances in this field. In summary, the performance of graphene-based EO/TO modulators on silicon photonics platform would be further improved with rapid developments of technology and they would then play increasingly important roles in a wide range of applications, including but not limited to telecom, computing, quantum information processing, and beam steering.

Funding

This work was supported by the National Key R&D Program of China (2019YFB2205204), the National Natural Science Foundation of China (61875120), and the "Shuguang Program" supported by Shanghai Education Development Foundation and Shanghai Municipal Education Commission.

Conflict of interest

The authors declare no conflict of interest.

References

1 Liu AS, Jones R, Liao L, *et al.* A high-speed silicon optical modulator based on a metal-oxide-semiconductor capacitor. *Nature* 2004; **427**: 615–618.

2 Thomson DJ, Gardes FY, Fedeli JM, *et al.* 50-Gb/s silicon optical modulator. *IEEE Photon Technol Lett* 2012; **24**: 234–236.

3 Chen A, Murphy E. *Broadband Optical Modulators: Science, Technology, and Applications*. Boca Raton: CRC Press, 2011.

4 Xu QF, Schmidt B, Pradhan S, *et al.* Micrometre-scale silicon electro-optic modulator. *Nature* 2005; **435**: 325–327.

5 Lu LJ, Zhao SY, Zhou LJ, *et al.* 16×16 non-blocking silicon optical switch based on electro-optic Mach-Zehnder interferometers. *Opt Express* 2016; **24**: 9295–9307.

6 Qiao L, Tang W, Chu T. 32 × 32 silicon electro-optic switch with built-in monitors and balanced-status units. *Sci Rep* 2017; **7**: 42306.

7 Zhou HL, Zhao YH, Wei YX, *et al.* All-in-one silicon photonic polarization processor. *Nanophotonics* 2019; **8**: 2257–2267.

8 Sharma J, Xuan Z, Li H, *et al.* Silicon photonic microring-based 4×112 Gb/s WDM transmitter with photocurrent-based thermal control in 28-nm CMOS. *IEEE J Solid-State Circuits* 2022; **57**: 1187–1198.

9 Ding JF, Chen HT, Yang L, *et al.* Ultra-low-power carrier-depletion Mach-Zehnder silicon optical modulator. *Opt Express* 2012; **20**: 7081–7087.

10 Gao G, Luo M, Li X, *et al.* Transmission of 286 Tb/s data stream in silicon subwavelength grating waveguides. *Opt Express* 2017; **25**: 2918–2927.

11 Li CL, Liu DJ, Dai DX. Multimode silicon photonics. *Nanophotonics* 2018; **8**: 227–247.

12 Blumenthal DJ, Heideman R, Geuzebroek D, *et al.* Silicon nitride in silicon photonics. *Proc IEEE* 2018; **106**: 2209–2231.

13 Miller SA, Chang YC, Phare CT, *et al.* Large-scale optical phased array using a low-power multi-pass silicon photonic platform. *Optica* 2020; **7**: 3–6.

14 Tang YB, Peters JD, Bowers JE. Over 67 GHz bandwidth hybrid silicon electroabsorption modulator with asymmetric segmented electrode for 13 μm transmission. *Opt Express* 2012; **20**: 11529–11535.

15 Xu H, Li XY, Xiao X, *et al.* High-speed silicon modulator with band equalization. *Opt Lett* 2014; **39**: 4839–4842.

16 Liao QW, Zhang YG, Ma SY, *et al.* A 50-Gb/s PAM-4 silicon-photonic transmitter incorporating lumped-segment MZM, distributed CMOS driver, and integrated CDR. *IEEE J Solid-State Circuits* 2022; **57**: 767–780.

17 Harris NC, Ma YJ, Mower J, *et al.* Efficient, compact and low loss thermo-optic phase shifter in silicon. *Opt Express* 2014; **22**: 10487–10493.

18 Fang Q, Song JF, Liow TY, *et al.* Ultralow power silicon photonics thermo-optic switch with suspended phase arms. *IEEE Photon Technol Lett* 2011; **23**: 525–527.

19 Nejadriahi H, Friedman A, Sharma R, *et al.* Thermo-optic properties of silicon-rich silicon nitride for on-chip applications. *Opt Express* 2020; **28**: 24951–24960.

20 Joo J, Park J, Kim G. Cost-effective 2×2 silicon nitride Mach-Zehnder interferometric (MZI) thermo-optic switch. *IEEE Photon Technol Lett* 2018; **30**: 740–743.

21 Geim AK. Graphene: Status and prospects. *Science* 2009; **324**: 1530–1534.

22 Novoselov KS, Fal'ko VI, Colombo L, *et al.* A roadmap for graphene. *Nature* 2012; **490**: 192–200.

23 Chen K, Zhou X, Cheng X, *et al.* Graphene photonic crystal fibre with strong and tunable light-matter interaction. *Nat Photonics* 2019; **13**: 754–759.

24 Sun Z, Martinez A, Wang F. Optical modulators with 2D layered materials. *Nat Photon* 2016; **10**: 227–238.

25 Jin M, Wei ZY, Meng YF, *et al.* Silicon-based graphene electro-optical modulators. *Photonics* 2022; **9**: 82.

26 Amin R, Ma ZZ, Maiti R, *et al.* Attojoule-efficient graphene optical modulators. *Appl Opt* 2018; **57**: D130–D140.

27 Koester SJ, Li M. High-speed waveguide-coupled graphene-on-graphene optical modulators. *Appl Phys Lett* 2012; **100**: 171107.

28 Yang ZH, Lu RG, Cai SW, *et al.* A CMOS-compatible and polarization-insensitive graphene optical modulator. *Optics Commun* 2019; **450**: 130–135.

29 Hu X, Zhang YG, Chen DG, *et al.* Design and modeling of high efficiency graphene intensity/phase modulator based on ultra-thin silicon strip waveguide. *J Lightwave Technol* 2019; **37**: 2284–2292.

30 Hu X, Long Y, Ji MX, *et al.* Graphene-silicon microring resonator enhanced all-optical up and down wavelength conversion of QPSK signal. *Opt Express* 2016; **24**: 7168–7177.

31 Du X, Skachko I, Barker A, *et al.* Approaching ballistic transport in suspended graphene. *Nat Nanotech* 2008; **3**: 491–495.

32 Bao QL, Loh KP. Graphene photonics, plasmonics, and broadband optoelectronic devices. *ACS Nano* 2012; **6**: 3677–3694.

33 Pan T, Qiu CY, Wu JY, *et al.* Analysis of an electro-optic modulator based on a graphene-silicon hybrid 1D photonic crystal nanobeam cavity. *Opt Express* 2015; **23**: 23357–23364.

34 Sorianello V, Contestabile G, Midrio M, *et al.* Chirp management in silicon-graphene electro absorption modulators. *Opt Express* 2017; **25**: 19371–19381.

35 Qiu CY, Gao WL, Vajtai R, *et al.* Efficient modulation of 1.55 μm radiation with gated graphene on a silicon microring resonator. *Nano Lett* 2014; **14**: 6811–6815.

36 Nair RR, Blake P, Grigorenko AN, *et al.* Fine structure constant defines visual transparency of graphene. *Science* 2008; **320**: 1308.

37 Schall D, Mohsin M, Sagade AA, *et al.* Infrared transparent graphene heater for silicon photonic integrated circuits. *Opt Express* 2016; **24**: 7871–7878.

38 Yan SQ, Zhu XL, Frandsen LH, *et al.* Slow-light-enhanced energy efficiency for graphene microheaters on silicon photonic crystal waveguides. *Nat Commun* 2017; **8**: 14411.

39 Xu ZZ, Qiu CY, Yang YX, *et al.* Ultra-compact tunable silicon nanobeam cavity with an energy-efficient graphene micro-heater. *Opt Express* 2017; **25**: 19479–19486.

40 Liu M, Yin XB, Ulin-Avila E, *et al.* A graphene-based broadband optical modulator. *Nature* 2011; **474**: 64–67.

41 Hu YT, Pantouvaki M, Van Campenhout J, *et al.* Broadband 10 Gb/s operation of graphene electro-absorption modulator on silicon. *Laser Photonics Rev* 2016; **10**: 307–316.

42 Sorianello V, Contestabile G, Midrio M, *et al.* Optical pre-emphasis by cascaded graphene electro absorption modulators. *IEEE Photon Technol Lett* 2019; **31**: 955–958.

43 Liu M, Yin XB, Zhang X. Double-layer graphene optical modulator. *Nano Lett* 2012; **12**: 1482–1485.

44 Mohsin M, Schall D, Otto M, *et al.* Graphene based low insertion loss electro-absorption modulator on SOI waveguide. *Opt Express* 2014; **22**: 15292–15297.

45 Youngblood N, Anugrah Y, Ma R, *et al.* Multifunctional graphene optical modulator and photodetector integrated on silicon waveguides. *Nano Lett* 2014; **14**: 2741–2746.

46 Dalir H, Xia Y, Wang Y, *et al.* Athermal broadband graphene optical modulator with 35 GHz speed. *ACS Photonics* 2016; **3**: 1564–1568.

47 Giambra MA, Sorianello V, Miseikis V, *et al.* High-speed double layer graphene electro-absorption modulator on SOI waveguide. *Opt Express* 2019; **27**: 20145–20155.

48 Sorianello V, Midrio M, Contestabile G, *et al.* Graphene-silicon phase modulators with gigahertz bandwidth. *Nat Photon* 2018; **12**: 40–44.

49 Ding YH, Zhu XL, Xiao SS, *et al.* Effective electro-optical modulation with high extinction ratio by a graphene-silicon microring resonator. *Nano Lett* 2015; **15**: 4393–4400.

50 Phare CT, Lee YHD, Cardenas J, *et al.* Graphene electro-optic modulator with 30 GHz bandwidth. *Nat Photon* 2015; **9**: 511–514.

51 Lee BS, Kim B, Freitas AP, *et al.* High-performance integrated graphene electro-optic modulator at cryogenic temperature. *Nanophotonics* 2020; **10**: 99–104.

52 Heidari E, Dalir H, Koushyar FM, *et al.* Integrated ultra-high-performance graphene optical modulator. *Nanophotonics* 2022; **11**: 4011–4016.

53 Majumdar A, Kim J, Vuckovic J, *et al.* Electrical control of silicon photonic crystal cavity by graphene. *Nano Lett* 2013; **13**: 515–518.

54 Gan XT, Shiue RJ, Gao YD, *et al.* High-contrast electrooptic modulation of a photonic crystal nanocavity by electrical gating of graphene. *Nano Lett* 2013; **13**: 691–696.

55 Gao YD, Shiue RJ, Gan XT, *et al.* High-speed electro-optic modulator integrated with graphene-boron nitride heterostructure and photonic crystal nanocavity. *Nano Lett* 2015; **15**: 2001–2005.

56 Sun TB, Kim JW, Yuk JM, *et al.* Surface-normal electro-optic spatial light modulator using graphene integrated on a high-contrast grating resonator. *Opt Express* 2016; **24**: 26035–26043.

57 Wang H, Zhou J, Song DF, *et al.* Active tuning of near-infrared electromagnetic responses in the graphene/silicon hybrid nanohole arrays by electrical control. *Phys Rev B* 2022; **105**: 035407.

58 Gan S, Cheng CT, Zhan YH, *et al.* A highly efficient thermo-optic microring modulator assisted by graphene. *Nanoscale* 2015; **7**: 20249–20255.

59 Nakamura S, Sekiya K, Matano S, *et al.* High-speed and on-chip optical switch based on a graphene microheater. *ACS Nano* 2022; **16**: 2690–2698.

60 Yu LH, Yin YL, Shi YC, *et al.* Thermally tunable silicon photonic microdisk resonator with transparent graphene nanoheaters. *Optica* 2016; **3**: 159–166.

61 Ma YQ, Li JH, Han ZH, *et al.* All-dielectric graphene-induced T-Slot waveguide electro-optic modulator with polarization-independent operation. *IEEE J Sel Top Quantum Electron* 2021; **27**: 3400708.

62 Chen W, Fan XJ, Li PF, *et al.* Polarization-insensitive electro-absorption modulator based on graphene-silicon nitride hybrid waveguide. *IEEE Photonics J* 2021; **13**: 6600213.

63 Mao D, Cheng C, Wang FF, *et al.* Device architectures for low voltage and ultrafast graphene integrated phase modulators. *IEEE J Sel Top Quantum Electron* 2021; **27**: 3400309.

64 Ji LT, Zhang DM, Xu Y, *et al.* Design of an electro-absorption modulator based on graphene-on-silicon slot waveguide. *IEEE Photonics J* 2019; **11**: 7800911.

65 Alessandri C, Asselberghs I, Brems S, *et al.* 5×25 Gbit/s WDM transmitters based on passivated graphene-silicon electro-absorption modulators. *Appl Opt* 2020; **59**: 1156.

66 Sorianello V, Contestabile G, Romagnoli M. Graphene on silicon modulators. *J Lightwave Technol* 2020; **38**: 2782–2789.

67 Denoyer G, Cole C, Santipo A, *et al.* Hybrid silicon photonic circuits and transceiver for 50 Gb/s NRZ transmission over single-mode fiber. *J Lightwave Technol* 2015; **33**: 1247–1254.

68 Barclay PE, Srinivasan K, Painter O. Nonlinear response of silicon photonic crystal micresonators excited via an integrated waveguide and fiber taper. *Opt Express* 2005; **13**: 801–820.

69 Ludwig GW, Watters RL. Drift and conductivity mobility in silicon. *Phys Rev* 1956; **101**: 1699–1701.

70 Krückel CJ, Torres-Company V, Andrekson PA, *et al.* Continuous wave-pumped wavelength conversion in low-loss silicon nitride waveguides. *Opt Lett* 2015; **40**: 875–878.

71 Arbabi A, Goddard LL. Measurements of the refractive indices and thermo-optic coefficients of Si_3N_4 and SiO_x using microring resonances. *Opt Lett* 2013; **38**: 3878–3881.

72 Ziegler G, Heinrich J, Wötting G. Relationships between processing, microstructure and properties of dense and reaction-bonded silicon nitride. *J Mater Sci* 1987; **22**: 3041–3086.

73 Leitch S, Moewes A, Ouyang L, *et al.* Properties of non-equivalent sites and bandgap of spinel-phase silicon nitride. *J Phys-Condens Matter* 2004; **16**: 6469–6476.

74 Kalli K, Dobb HL, Webb DJ, *et al.* Development of an electrically tuneable Bragg grating filter in polymer optical fibre operating at 1.55 μm. *Meas Sci Technol* 2007; **18**: 3155–3164.

75 Takahashi M, Uchida Y, Yamasaki S, *et al.* Compact and low-loss coherent mixer based on high Δ ZrO_2-SiO_2 PLC. *J Lightwave Technol* 2014; **32**: 3081–3088.

76 Soref RA, Bennett BR. Electrooptical effects in silicon. *IEEE J Quantum Electron* 1987; **23**: 123–129.

77 Zhan D, Yan JX, Lai LF, *et al.* Engineering the electronic structure of graphene. *Adv Mater* 2012; **24**: 4055–4069.

78 Avouris P. Graphene: Electronic and photonic properties and devices. *Nano Lett* 2010; **10**: 4285–4294.

79 Cano D, Ferrier A, Soundarapandian K, *et al.* Fast electrical modulation of strong near-field interactions between erbium emitters and graphene. *Nat Commun* 2020; **11**: 4094.

80 Sherrott MC, Hon PWC, Fountaine KT, *et al.* Experimental demonstration of >230° phase modulation in gate-tunable graphene-gold reconfigurable mid-infrared metasurfaces. *Nano Lett* 2017; **17**: 3027–3034.

81 Kim J, Son H, Cho DJ, *et al.* Electrical control of optical plasmon resonance with graphene. *Nano Lett* 2012; **12**: 5598–5602.

82 Yin X, Ke XM, Chen L, *et al.* Ultra-broadband TE-pass polarizer using a cascade of multiple few-layer graphene embedded silicon waveguides. *J Lightwave Technol* 2016; **34**: 3181–3187.

83 Pei CY, Yang LZ, Wang GC, *et al.* Broadband graphene/glass hybrid waveguide polarizer. *IEEE Photon Technol Lett* 2015; **27**: 927–930.

84 Bao QL, Zhang H, Wang B, *et al.* Broadband graphene polarizer. *Nat Photon* 2011; **5**: 411–415.

85 Du W, Li EP, Hao R. Tunability analysis of a graphene-embedded ring modulator. *IEEE Photon Technol Lett* 2014; **26**: 2008–2011.

86 Li H, Anugrah Y, Koester SJ, *et al.* Optical absorption in graphene integrated on silicon waveguides. *Appl Phys Lett* 2012; **101**: 111110.

87 Qiu CY, Pan T, Gao WL, *et al.* Proposed high-speed micron-scale spatial light valve based on a silicon-graphene hybrid structure. *Opt Lett* 2015; **40**: 4480–4483.

88 Ye SW, Yuan F, Zou XH, *et al.* High-speed optical phase modulator based on graphene-silicon waveguide. *IEEE J Sel*

Top Quantum Electron 2017; **23**: 76–80.

89 Tao YS, Shu HW, Jin M, *et al.* Numerical investigation of the linearity of graphene-based silicon waveguide modulator. *Opt Express* 2019; **27**: 9013–9031.

90 Sorianello V, Midrio M, Romagnoli M. Design optimization of single and double layer graphene phase modulators in SOI. *Opt Express* 2015; **23**: 6478–6490.

91 Rodriguez FJ, Aznakayeva DE, Marshall OP, *et al.* Solid-state electrolyte-gated graphene in optical modulators. *Adv Mater* 2017; **29**: 1606372.

92 Zeng BB, Huang ZQ, Singh A, *et al.* Hybrid graphene metasurfaces for high-speed mid-infrared light modulation and single-pixel imaging. *Light Sci Appl* 2018; **7**: 51.

93 Yu LH, Dai DX, He SL. Graphene-based transparent flexible heat conductor for thermally tuning nanophotonic integrated devices. *Appl Phys Lett* 2014; **105**: 251104.

94 Kim JT, Chung KH, Choi CG. Thermo-optic mode extinction modulator based on graphene plasmonic waveguide. *Opt Express* 2013; **21**: 15280–15286.

95 Su MY, Yang B, Liu JM, *et al.* Broadband graphene-on-silicon modulator with orthogonal hybrid plasmonic waveguides. *Nanophotonics* 2020; **9**: 1529–1538.

96 Wang BB, Blaize S, Seok JB, *et al.* Plasmonic-based subwavelength graphene-on-hBN modulator on silicon photonics. *IEEE J Sel Top Quantum Electron* 2019; **25**: 4600706.